Comparison of amorphous Fe-S-O and crystalline FeS_2 pyrite for photovoltaic application

Shoichi Kawai, Takahiro Kajima and Masaya Ichimura

Department of Engineering Physics, Electronics, and Mechanics., Nagoya Institute of Technology, Gokiso, Showa, Nagoya, Aichi, 466-8555 Japan
DESO CORP. Research Laboratories, 500-1 Minamiyama, Komenoki, Nissin, Aichi, 470-0111 Japan

Abstract
Iron sulfide oxide thin films were deposited by electrochemical deposition and annealed with sulfur powder. The composition ratio of the as-deposited film is Fe:S:O = 1: 1.5: 0.4. X-ray diffraction (XRD) and Raman measurement results showed that the as-deposited film is amorphous. After the annealing at 400ºC with sulfur powder, oxygen content was significantly reduced, and crystallization of FeS_2 pyrite was confirmed by XRD. Heterojunction cells were fabricated using both the as-deposited and annealed films with ZnO thin film as the partner, and rectification properties were confirmed for all the samples. However, the leakage current was increased and the forward current was decreased by the annealing. Thus, the as-deposited amorphous film seems to be more suited for photovoltaic application than the annealed ones.

keywords: iron sulfide, iron oxide, pyrite, electrochemical deposition

1. Introduction

Iron pyrite (FeS_2) has attracted considerable attention as an earth-abundant and nontoxic material well suited for photovoltaic and photo-electrochemical applications [1]. Pyrite FeS_2 has a bandgap energy of 0.95 eV and a high optical absorption coefficient ($\alpha \gg 5 \times 10^5$ cm^{-1}) in the visible range [2]. Owing to this high absorption coefficient, a very thin film (< 1μm) is sufficient for absorbing most of the incident solar radiation, and thus FeS2 has even larger electricity generation potential than Si, for which a much larger thickness (> 100 μm) is needed for sufficient photo absorption [3]. So far, FeS_2 bulk crystals and thin films were fabricated by various techniques, such as chemical vapor transport [2,4], sulfurization of iron films [5-7], metal organic chemical vapor deposition [8-10], low pressure chemical vapor deposition [11], spray pyrolysis [12], electrochemical deposition (ECD) [13-17], sulfurization of an iron molecular ink [18], and laser annealing of a multiphase iron sulfide film [19]. Nevertheless, there is no report of successful fabrication of a heterojunction solar cell based on FeS_2. Recently, a few groups reported fabrication of diodes based on FeS_2 nano particles [20-22]. On the other hand, fabrication of pn junction diodes has not been reported for single- or poly-crystalline FeS_2 fabricated by conventional techniques. The reason for the failure is not well understood. Presence of impurity phases such as marcasite and mono sulfide is generally regarded as one possible reason. Both marcasite and mono sulfide have a much smaller band gap (<0.3 eV) than that of pyrite, and thus will act as a shunt path in the diode structure. Another possible reason is high-density of native defects in bulk and surface of pyrite [20,21,23,24].

In previous works, we reported ECD of iron-sulfide-oxide (Fe-S-O) films [25, 26]. The as-deposited films are amorphous and contain significant amount of oxygen. We also fabricated pn heterojunctions with ZnO using as-deposited Fe-S-O films, and confirmed rectification properties. ECD of FeS_2 has been attempted by several other groups as noted above; they all annealed deposited films in sulfur ambient before characterization, and none of them reported fabrication of pn junction devices. Thus, it is necessary to clarify impact of the annealing on the properties of the Fe-S-O films, i.e., whether the annealing can improve or deteriorate the properties. In this work, we deposit Fe-S-O films by ECD and anneal them in sulfur atmosphere. Heterojunctions with ZnO are fabricated for both the as-deposited and annealed films, and effects of the annealing on properties of the heterojuctions are investigated. On the basis of these results, we discuss which is more suitable for photovoltaic application, the as-deposited amorphous film or the annealed crystalline film.

2. Experiments

A three-electrode cell was used for ECD with a saturated calomel electrode (SCE) as the reference electrode. Indium-tin-oxide (ITO)-coated glass was used as the working electrode (substrate) and a platinum sheet as the counter electrode. Hokuto denko function

generator HB-305 and potentiostat/ galvanostat HA-151B were used as the voltage source. The ITO substrate was washed ultrasonically in acetone and dried in nitrogen before the experiment. The deposition area was about 1x1 cm^2. The aqueous electrolyte solution for the deposition contained 30 mM $FeSO_4$ and 100 mM $Na_2S_2O_3$, and the solution pH was unadjusted (about 4.5), and solution temperature was adjusted to 15 ºC by a cool stirrer [25]. The deposition potential was -1.0 V vs. SCE, and the deposition time was 1.5 min. Immediately after the deposition, the deposited sample was dried by the nitrogen gas. (The deposited sample was oxidized and its color changed to yellow when it was left for one day after the deposition without drying.)

For the sulfur annealing, the sample with 30 mg sulfur powder placed on it was sandwiched between two glass plates and wrapped in aluminum foil [27]. Then, it was placed in an electric furnace, and after evacuation for 10 min by a rotary pump, it was annealed at 300ºC and 400ºC for one hour. Separate Fe-S-O samples were prepared under the same condition for characterization before the annealing and after the annealing at each temperature, and also for fabrication of heterostructures.

The heterojunction structure was fabricated by depositing ZnO by ECD on both the as-deposited and sulfur-annealed films. The film thickness was about 1 μm, and the ZnO deposition area was 6×6 mm^2. ECD of ZnO was carried out using an aqueous solution containing 100 mM $Zn(NO_3)_2$ [28, 29]. The pH of the solution was not adjusted (about 4). The electrolyte temperature was kept at 60°C throughout the deposition, the deposition current density was -11 mA/cm^2, and the deposition time was 1.5 min. Indium metal was evaporated on ZnO to form contact electrodes of 1x1 mm^2 size.

The film thickness was measured by a profile meter Accretech, Surfcom-1400D. The compositional analysis was carried out by Auger electron spectroscopy (AES) using the model JEOL JAMP 9500F. The film morphology was also investigated by field emission scanning electron microscope (SEM) using JEOL JAMP 9500F. Photoelectrochemical (PEC) measurements were carried out in an aqueous electrolyte containing 100 mM $Na_2S_2O_3$. The applied voltage was swept at a speed of 5 mV/s, and the illumination was switched on and off each 5 s. A xenon lamp (100 mW/cm^2) was used as a light source. X-ray diffraction (XRD) patterns were recorded with the BRUKER D8 DISCOVER diffractometer using CuKa radiation at the grazing-angle 5° of incident X-ray. Current-voltage (J-V) characteristics of the heterostructures were measured in the dark.

3. Results and discussion

The deposited Fe-S-O film was black, compact, and about 0.3 μm in thickness. Fig. 1 shows the SEM surface images and the thickness profiles of the as-deposited and annealed films. By the annealing, surface roughness was reduced while the thickness was not affected significantly.

Figure 2 (a) shows the AES spectra for the as-deposited and annealed samples, and the

elemental compositions obtained from them are plotted in Fig. 2(b). The spectra were taken at several points on the surface for each sample, and the average values were plotted in Fig. 2(b). The error bars indicate range of distribution within each sample. For the as-deposited film, the composition is Fe:S:O = 1 : 1.5 : 0.4, and thus the oxygen content is comparable to the sulfur content. By the 400°C-annealing, the S/Fe ratio increased from 1.5 to 2.4, and the O/Fe ratio decreased from 0.4 to 0.1.

Figure 3 shows the XRD measurement results for the as-deposited and annealed samples. The peaks due to ITO are labeled with "*", while the peaks which can be assigned to FeS_2 pyrite are indexed. For the as-deposited film, only the peaks due to ITO were observed. Thus, the as-deposited film is amorphous, and the elemental iron or sulfur phase do not seem to be included. After the 300ºC-annealing, the (200) peak of pyrite is observed. The pyrite peaks of (111), (200), (210), (211), (220) and (311) were observed for the 400°C-annealed film.

Figure 4 shows the Raman spectra of the as-deposited and sulfur-annealed films. The as-deposited film exhibited a broad signal ranging from 320 to 400 cm^{-1}, which indicates amorphous nature of the film. Small humps appear around 340 and 380 cm^{-1} and may be attributed to bonding as in the pyrite phase [30], whereas another hump at 325 cm^{-1} could be attributed to the marcasite-like bonding [31]. It should be noted that Raman scattering can be observed even for amorphous materials, while the long-range atomic ordering is necessary for X-ray diffraction. Thus, the as-deposited film is thought to be amorphous but retain the local bonding configuration corresponding to FeS_2 (pyrite or marcasite), which results in the observed Raman signal. The amorphous nature of the film seems to cause the broadening and shift of the peaks. After the 300ºC-annealing, the humps around 340 and 380cm^{-1} became two peaks. The 400ºC-annealed films exhibited clear peaks at 342, 378 and 425 cm^{-1} attributed to the pyrite phase. However, there is additional peak at 325 cm^{-1} attributed to the marcasite phase. Thus, the results of XRD and Raman show that the film is initially amorphous and after the 400°C-annealing crystallizes dominantly as pyrite but includes the minor marcasite phase.

Figure 5 shows the optical transmission spectra for the as-deposited and annealed films. For the as-deposited film, the transmission is less than 10 % in the entire wavelength range and decreases gradually with decreasing wavelength. The annealed samples exhibit more abrupt change in the transmission; the transmission is lower than for the as-deposited sample in the short wavelength range (< 1 μm) and higher in the long wavelength range (> 1.1 μm). The absorption edge is still not clear for the 300ºC-annealed sample, while the edge seems to appear around 1.1 μm for the 400ºC annealed sample. The dependence of the absorption coefficient (α) on the photon energy ($h\nu$) is known to be given by the equation $\alpha h\nu \propto (h\nu - E_g)^n$, where E_g is the band gap and the exponent n = 1/2 for allowed direct transition and n = 2 for allowed indirect transition. In order to estimate a band gap for the 400ºC-annealed sample, $(\alpha h\nu)^n$ (n=2, 1/2) is plotted in Fig. 6 against $h\nu$ [32, 33]. However, there is no clear straight line portion in the plot. The direct band gap is roughly estimated to be in a range of 0.9 ~ 1.2

eV from the $(\alpha h\nu)^2$ plot, while the indirect band gap estimated from the $(\alpha h\nu)^{1/2}$ plot seems to be in a range of 0.6 ~ 0.8 eV. The direct band gap is not largely different from the literature value of the band gap of pyrite (0.95 eV), whereas the indirect band gap is smaller than it.

The conduction type and photo sensitivity were investigated by the PEC measurement. Figure 7 shows the PEC measurement results for the as-deposited and sulfur annealed films. In the PEC measurement, a current due to minority carriers is enhanced by illumination. In Fig 7, the as-deposited film showed small negative photocurrent, and therefore, the minority carrier is electron, i.e., the as-deposited film is p-type. On the other hand, both the 300°C and 400°C-annealed films did not show photocurrent. In the positive potential range, the films were unstable and the PEC data were not obtained.

The ZnO films deposited were polycrystalline and exhibited clear n-type conductivity [34, 35]. Figure 8 shows the results of the J-V measurement in the dark for the heterojunction cells with ZnO. Although all the cells exhibited rectification properties, rectification properties were deteriorated by the annealing: the leakage current was increased and the forward current density was decreased with increasing annealing temperature. According to the thickness profile data shown in Fig. 1, the surface roughness of the Fe-S-O film (the underlying layer) is larger for the as-deposited film than for the annealed films. Thus the heterointerface is also expected to be more rough for the as-deposited sample. In general, interface roughness increases the effective junction area and the numbers of grains (grain boundaries) included in the interface region, and thus can increase leakage current. However, the leakage current is in fact larger for the annealed samples, which are expected to have a more flat and smooth interface. Thus, the interface morphology will not be the dominant factor influencing the rectification properties. We can consider instead the following two reasons for the deterioration of rectification properties by the annealing. One is the change in conduction type by the annealing. In the PEC measurement, p-type response was observed for the as-deposited film and not for the annealed films. Thus, although the as-deposited film is p-type, the annealed films may not be clear p-type. Therefore, for the annealed films, a pn junction was not formed with ZnO, and rectification became poor. Another possible reason is a high defect density of the annealed samples. The absence of photocurrent in the PEC measurement indicates that the carrier lifetime is very short because of high density of deep levels working as recombination centers in the annealed samples. Such deep levels will enhance leakage current and thus deteriorate rectification properties of a pn junction. The forward current density is smaller for the annealed films, which indicates that resistivity was increased by the annealing. This may also be due to the deep levels.

As noted in Introduction, growth of crystalline FeS_2 pyrite has been attempted by many other groups, but successful fabrication of pn junction diodes based on it has never been reported. In this study, we have shown that the photo response in the PEC measurement is higher for the as-deposited film than for the annealed films. Moreover, the heterojunction based on the as-deposited film showed better diode properties than those based on the

annealed films. Those present and previous results indicate that the as-deposited film is more suited for photovoltaic application than the annealed crystalline film. It is generally agreed that synthesized FeS_2 pyrite often includes impurity phases such as marcasite and mono sulfide. On the other hand, the as-deposited amorphous Fe-S-O film is considered to be of single phase rather than a mixture of different phases. This could be the reason why the as-deposited film shows better electrical properties than the annealed films.

4. Conclusion

Fe-S-O thin films were fabricated by ECD and annealed with sulfur powder. The as-deposited film was amorphous, and its elemental composition is Fe:S:O = 1 : 1.5 : 0.4. After the 400°C-sulfur annealing, the composition ratio was Fe:S:O = 1 : 2.4 : 0.1 and pyrite peaks were observed in X-ray diffraction and Raman measurements. However, the marcasite peak was also observed in the Raman measurement. In the PEC measurement, although p-type photocurrent response was observed for the as-deposited film, no photo-response was observed for the annealed films. The heterostructures with ZnO were fabricated, and rectification properties were confirmed for both the as-deposited and annealed films. However, the leakage current was increased and forward current decreased by the annealing. This indicates that as-deposited amorphous Fe-S-O films will be more suitable for solar cell applications than the annealed, crystallized films.

Acknowledgments

This work was partly supported by ESPEC Foundation for Global Environment Research and Technology (Charitable Trust). We would like to thank Dr. Kato for his useful discussion.

References

[1] Altermatt P P, Kiesewetter T, Ellmer K and Tributsch H 2002 Sol. Energy Mater. Sol. Cells **71** 181

[2] Ennaoui A and Tributsch H 1986 Sol. Energy Mater. Sol. Cells **14** 461

[3] Wadia C, Alivisatos A P and Kammen D M 2009 Environ. Sci. Technol. **43** 2072

[4] Ennaoui A, Fiechter S, Pettenkofer Ch, Alonso-Vante N, Büker K, Höpfner Ch and Tributsch H 1993 Sol. Energy Mater. Sol. Cells **29** 289

[5] Meng L, Tu J P and Liu M S 1999 Mater. Lett. **38** 103

[6] Rezig B, Dahman H and Kenzari M 1992 Renewable Energy **2** 125

[7] Ferrer I J and Sanchez C 1999 J. Appl. Phys. **85** 7411

[8] Chatzietheodorou G, Fiechter S, Konenkamp R, Kunst M, Jaegermann W and Tributsch H 1986 Mater. Res. Bull. **21** 1481

[9] Hopfner C, Ellmer K, Ennaoui A, Pettenkofer C, Fiechter S and Tributsch H 1995 J. Cryst. Growth **151** 325

[10] Oertel J, Ellmer K, Bohne W, Rohrich J and Tributsch H 1999 J. Cryst. Growth **198/199** 1205

[11] M.Schleich D and Chang H S W 1991 J. Cryst. Growth **112** 737

[12] Yamamoto A, Nakamura M, Seki A, Li E L, Hashimoto A and Nakamura S 2003 Sol. Energy Mater. Sol. Cells **75** 451

[13] Nakamura S and Yamamoto A 2001 Sol. Energy Mater. Sol. Cells **65** 79

[14] Gomes A, Mendonça M H, Silva Pereira M I and Costa F M A 2000 J. Solid State Electrochemistry **4** 168

[15] Aricb A S, Pieruccini M, Monforte G, Antonucci V, Giordano N and Antonucci P L 1993 Mater. Chem. Phys. **34** 263

[16] Dong Y Z, Zheng Y F, Duan H, Sun Y F and Chen Y H 2005 Mater. Lett. **59** 2398

[17] Gomes A, Ares J R, Ferrer I J, Silva Pereira M I and Sanchez C 2003 Mater. Res. Bul. **38** 1123

[18] Seefeld S, Limpinsel M, Liu Y, Fa N, Farhi N, Weber A, Zhang Y N, Berry N, Kwon Y J, Perkins C L, Hemminger J C, Wu R Q and Law M 2013 J. Am. Chem. Soc. **135** 4412

[19] Umehara M, Takeda Y, Azuma H and Motohiro T 2012 Jpn. J. Appl. Phys. **51** 02BP10

[20] Steinhagen C, Harvey T B, Jackson Stolle C, Harris J and Korgel B A 2012 J. Phys. Chem. Lett. **3** 2352

[21] Wang D, Jiang Y, Lin C, Li S, Wang Y, Chen C and Chen C 2012 Adv. Mater. **24** 3415

[22] Moon D G, Cho A, Park J H, Ahn S H, Kwon H. S, Cho Y. S, Ahn S 2014 J. Mater. Chem. A **2** 17779

[23] Birkholz M, Fiechter S, Hartmann A and Tributsch H 1991 Phys. Rev. B, **43** 11926

[24] Bronold M, Pettenkofer C and Jaegermann W 1994 J. Appl. Phys. **76** 5800

[25] Kawai S, Yamazaki R, Sobue S, Okuno E and Ichimura M 2014 APL mater. **2** 032110

[26] Yang K, Kawai S and Ichimura M 2014 Thin Solid Films **573** 1
[27] Mazon-Montijo D A, Nair M T S and Nair P K 2013 ECS J. Solid St. Sci. Tech. **2** 465
[28] Izaki M 1997 J. Electrochem. Soc. **144** 1949
[29] Peulon S and Lincot D 1998 J. Electrochem. Soc. **145** 864
[30] Vogt H, Chattopadhyay T and Stolz H J 1983 J. Phys. Chem. Solids **44** 869
[31] Sourisseau C, Cavagnat R and Fouassier M 1991 J. Phys. Chem. Solids **52** 537
[32] Mohamed H A 2009 Eur. Phys. J. Appl. Phys. **48** 20504
[33] Ortega J J, Aguilar-Frutis M A, Alarcón G, Falcony C, Méndez-García V H, Araiza J J 2014 Mater. Sci. Eng. B **187** 83
[34] Ichimura M and Takagi H 2008 Jpn. J. Appl. Phys. **47** 7845
[35] Ichimura M and Song Y 2011 Jpn. J. Appl. Phys **50** 051002

Fig. 1 FE-SEM surface images and surface profiles of the as-deposited Fe-S-O film and those annealed in sulfur ambient at 300 and 400ºC.

Fig.2 (a) AES spectra of the as-deposited Fe-S-O film and those annealed in sulfur ambient at 300 and 400ºC, and (b) composition ratios (O/Fe and S/Fe) obtained from the AES spectra.

Fig. 3 Grazing-incidence (5º) X-ray diffraction patterns for the as-deposited Fe-S-O film and those annealed in sulfur ambient at 300 and 400ºC. The peaks due to ITO are marked with "*" while positions of the diffraction peaks of FeS_2 pyrite are shown by the dashed lines.

Fig. 4 Raman spectra of the as-deposited Fe-S-O film and those annealed in sulfur ambient at 300 and 400ºC. The peak wavenumbers of the dominant peaks of the 400ºC-annealed sample are noted in the figure.

Fig. 5 Optical transmission spectra for the as-deposited Fe-S-O film and those annealed in sulfur ambient at 300 and 400ºC.

Fig.6 Plot of the $(\alpha h\nu)^2$ vs $h\nu$ for the 400ºC annealed sample.

Fig. 7 PEC measurement results in a negative potential range for the as-deposited Fe-S-O film and those annealed in sulfur ambient at 300 and 400ºC. The step-like variation in the current is due to the chopped illumination.

Fig. 8 Dark J-V characteristics of the heterojunction cells with ZnO deposited on the as-deposited and annealed Fe-S-O films.

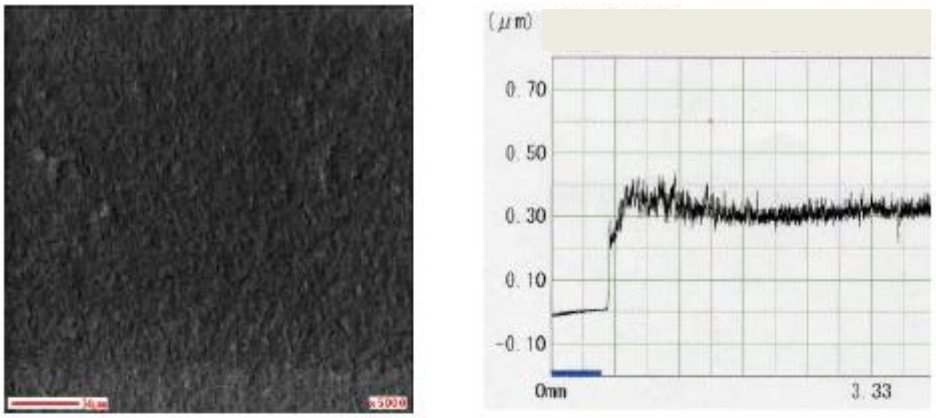

(a)As-deposited

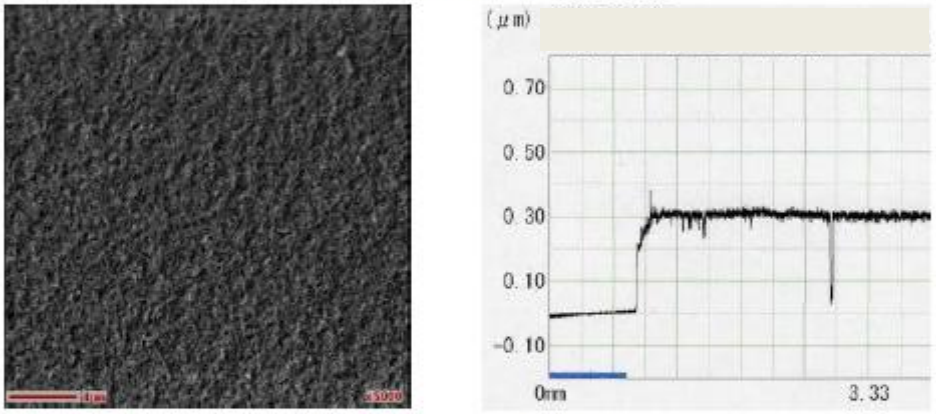

(b)300°C-annealed

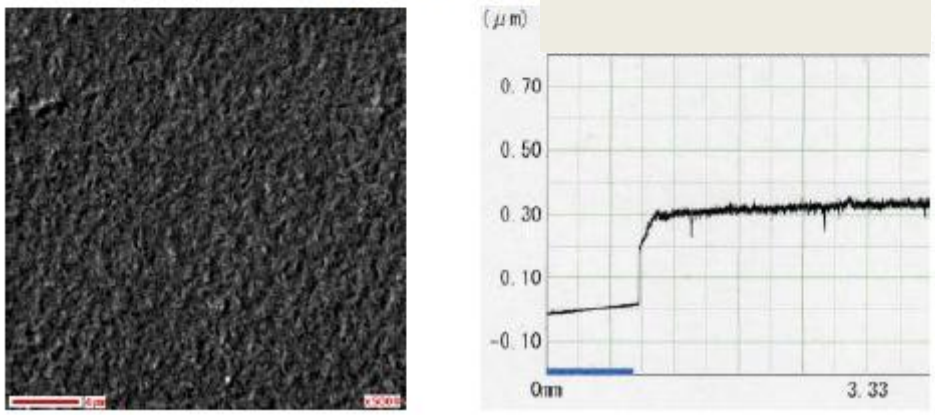

(c)400°C-annealed

Fig. 1

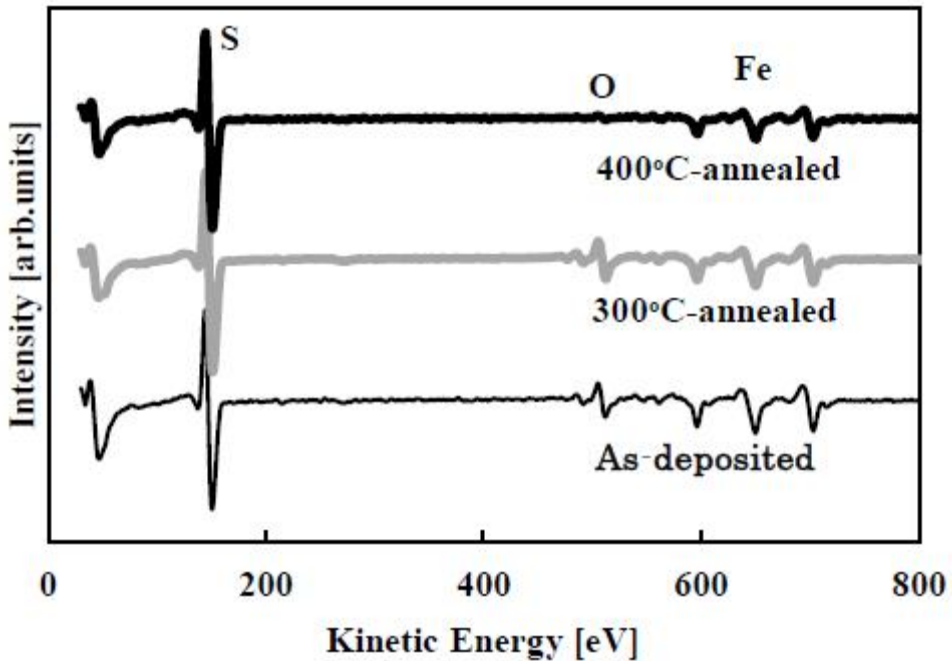
S
O
Fe
400°C-annealed
300°C-annealed
As-deposited
Intensity [arb.units]
0
200
400
600
800
Kinetic Energy [eV]

Fig.2 (a)

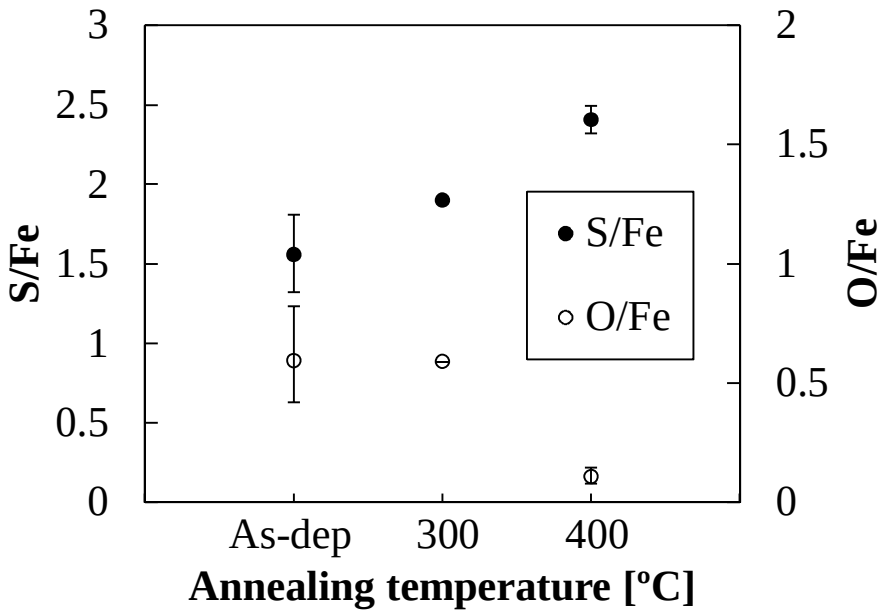
3
2.5
2
1.5
1
0.5
0
S/Fe
2
1.5
1
0.5
0
O/Fe
S/Fe
O/Fe
As-dep
300
400
Annealing temperature [°C]

Fig. 2(b)

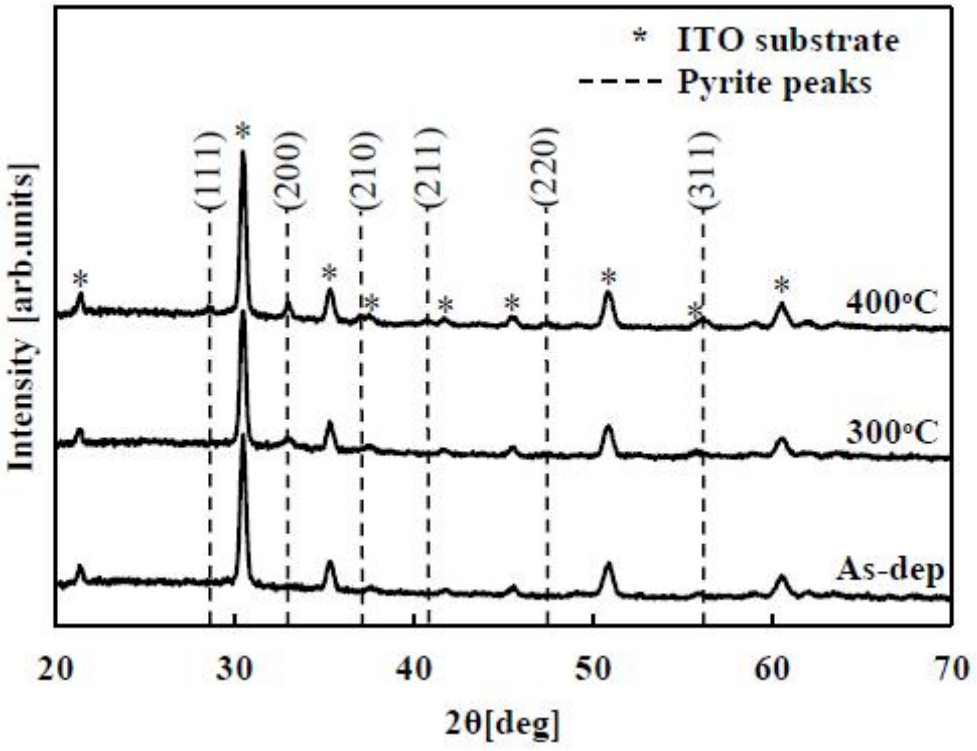
* ITO substrate
Pyrite peaks
(111)
(200)
(210)
(211)
(220)
(311)
400°C
300°C
As-dep
Intensity [arb.units]
20
30
40
50
60
70
2θ[deg]

Fig. 3

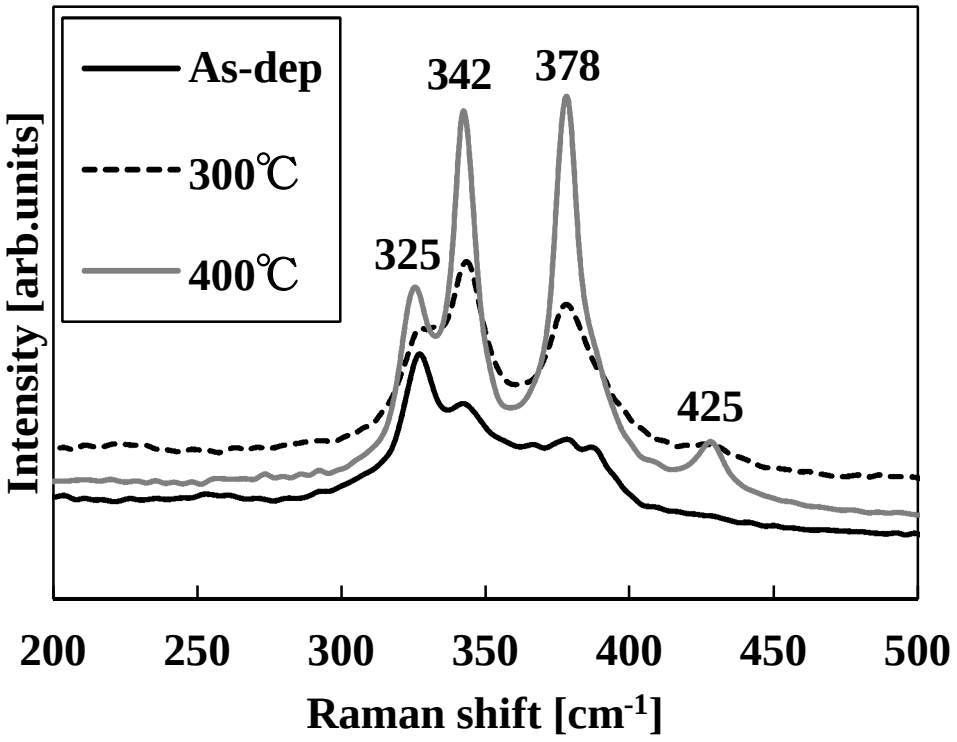
As-dep
300℃
400℃
342
378
325
425
Intensity [arb.units]
200
250
300
350
400
450
500
Raman shift [cm-1]

Fig. 4

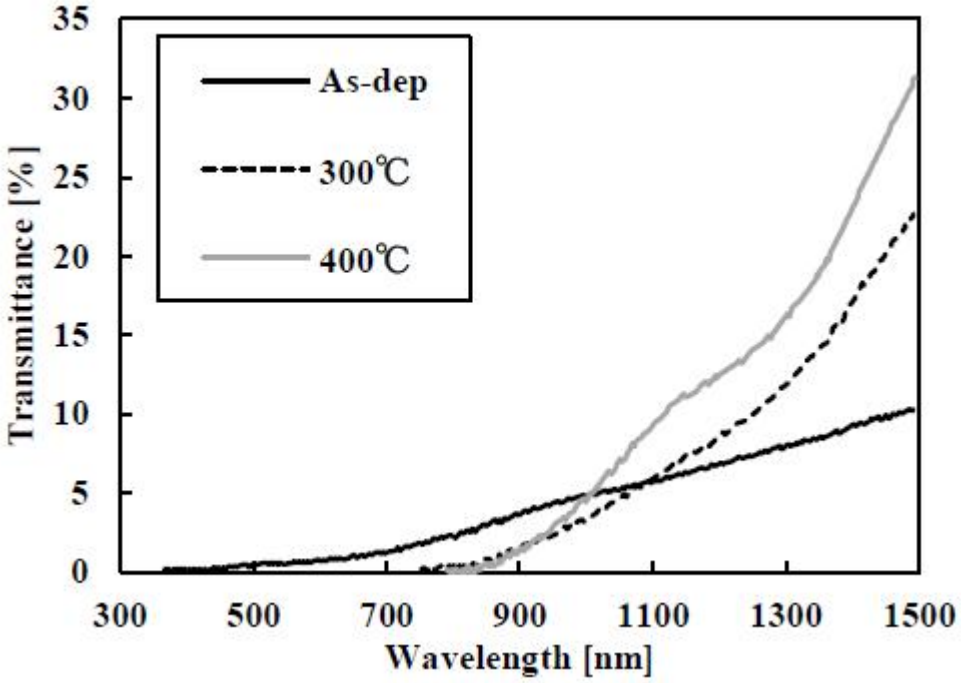
As-dep
300℃
400℃
Transmittance [%]
Wavelength [nm]
0
5
10
15
20
25
30
35
300
500
700
900
1100
1300
1500

Fig. 5

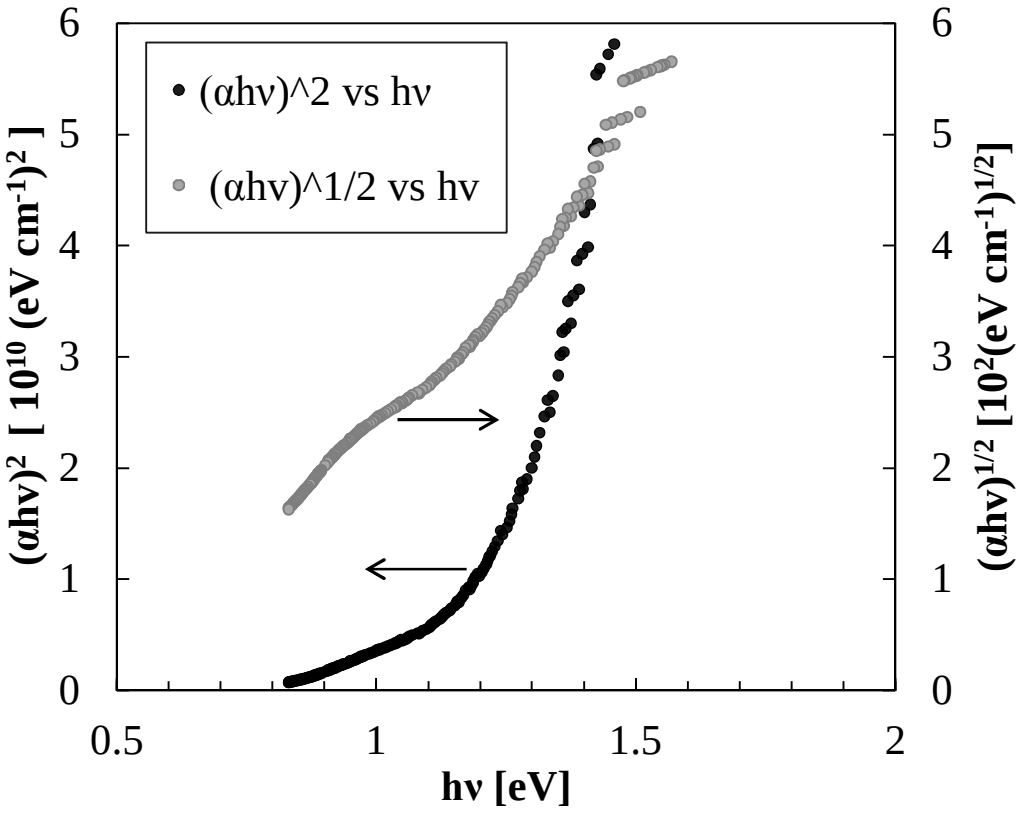
(αhν)^2 vs hν
(αhν)^1/2 vs hν
(αhν)² [10¹⁰ (eV cm⁻¹)²]
(αhν)^1/2 [10²(eV cm⁻¹)^1/2]
hν [eV]
0
1
2
3
4
5
6
0.5
1
1.5
2

Fig. 6

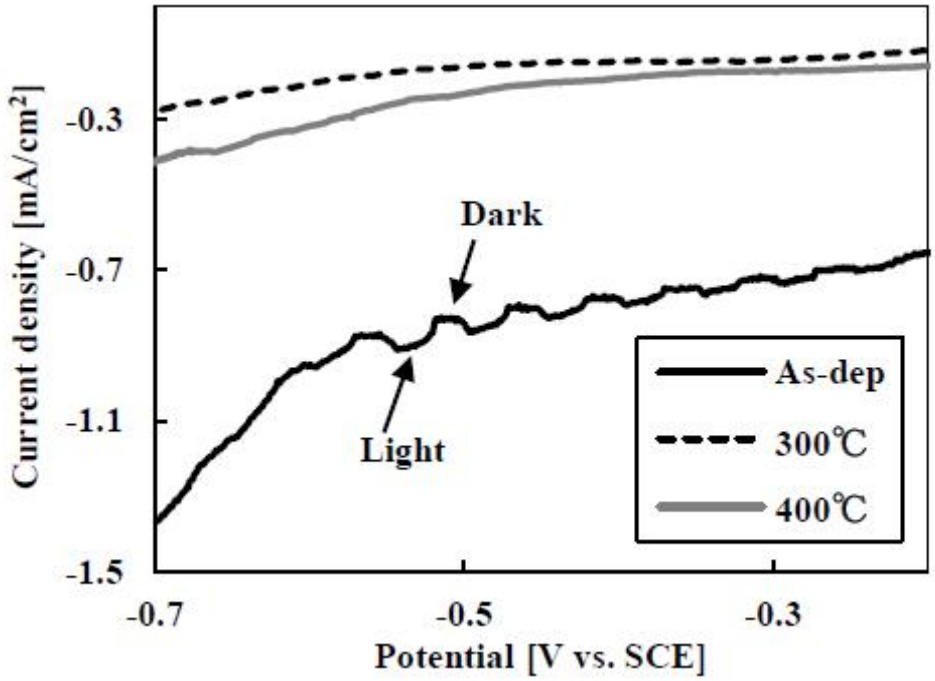
Current density [mA/cm²]
-0.3
-0.7
-1.1
-1.5
-0.7
-0.5
-0.3
Potential [V vs. SCE]
Dark
Light
As-dep
300℃
400℃

Fig.7

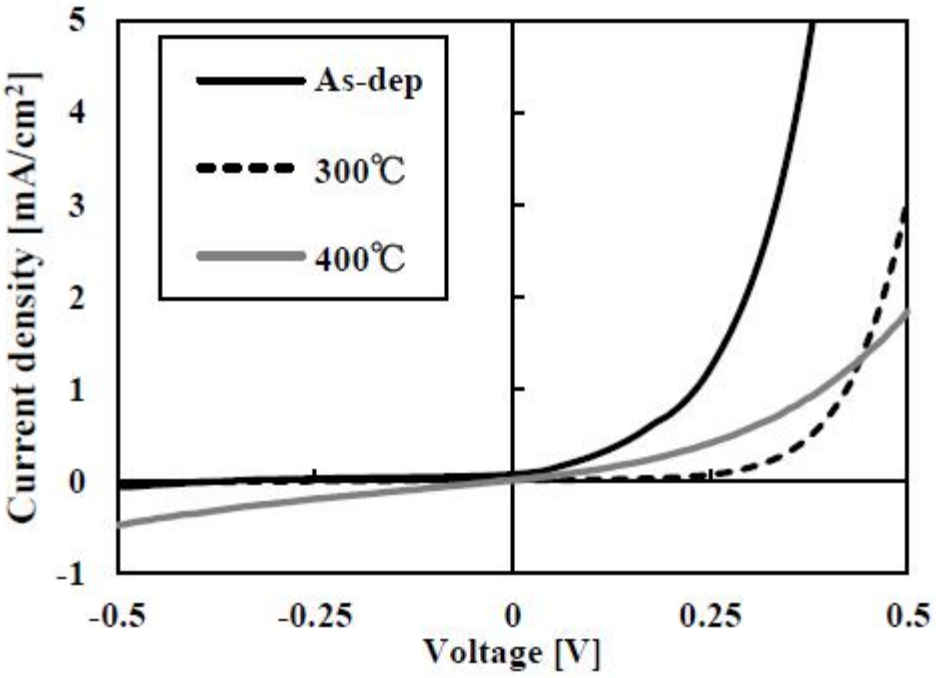
As-dep
300℃
400℃
Current density [mA/cm²]
5
4
3
2
1
0
-1
-0.5
-0.25
0
0.25
0.5
Voltage [V]

Fig.8